Joint EUROGRAPHICS - IEEE TCVG Symposium on Visualization (2003)
G.-P. Bonneau, S. Hahmann, C. D. Hansen (Editors)

Shrouds: Optimal Separating Surfaces for Enumerated Volumes

Gregory M. Nielson, Gary Graf, Ryan Holmes, Adam Huang, and Mariano Phielipp

Computer Science and Engineering, Arizona State University

Abstract

We describe new techniques for computing a smooth triangular mesh surface that surrounds an enumerated volume consisting of a collection of points from a 3D rectilinear grid. The surface has the topology of an isosurface computed by a marching cubes method applied to a field function that has the value one at the points in the volume and zero for points not in the volume. The vertices are confined to the edges of the grid that penetrate this separating surface and the precise positions are computed so as to optimize a certain energy functional applied to the surface. We use efficient iterative methods to compute the optimal separating surfaces. We lift the concept of energy functionals for planar curves to isosurfaces by means of the 4-network which is a unique collection of orthogonal planar polygons lying on the isosurface. The general strategy that we describe here leads to methods that are simple, efficient, and effective.*

1. Introduction

The techniques of this paper fall into the general topic of triangular mesh fairing [3, 12, 20, 21, 22]. Given a triangulated surface, the goal is to alter the geometry, topology or both to improve upon the surface by making it smoother. The smoothing criterion is prescribed by the desire to optimize a specified energy functional. Examples include the Dirichlet energy functional

$$|S| = \int |\nabla S|^2$$

and the thin plate functional

$$|S| = \int (k_1(S))^2 + (k_2(S))^2$$

where $k_1(S)$ and $k_2(S)$ are the principal curvatures being the eigenvalues of the shape operator [7]. Strategies for solving these optimization problems usually follow in the spirit of numerical methods for solving PDEs. Either finite element methods are applied directly to the energy functional or finite difference schemes are applied to the variational characterization provided by Euler-Lagrange equation. Typically this leads to sparse linear systems of equations which are solved iteratively. Since the Euler-Lagrange equation for the Dirichlet functional is the well-known Laplace equation, it is possible to exploit this connection for the development of surface fairing algorithms [24]. For the present context, there is an additional complication in that there is usually no explicit parameterization of the triangular mesh surface. This is what makes the problem interesting. Much of the recent research in this area has centered around the development of discrete approximations or characterizations which are independent of or do not require a parameterization of the triangular mesh surface. In fact, computable discrete approximations to energy functions or the variation (Fréchet derivatives) of these functionals can lead to algorithms for computing parameterizations themselves. Examples include the discrete conformal parameterization [20] and discrete authalic parameterization [4]. Dyn et al. [5] have used discrete approximations of Gaussian and mean curvature to fair triangular mesh surface with only topology changes based upon edge swapping schemes.

Here, we present methods that are quite different from the above, but they only apply to the restricted set of isosurfaces [19] computed with a marching cubes (mc) type of algorithm. Before we proceed to describe our optimization strategy, we motivate our application. The examples and applications of Section 4 further explain the purpose of this research.

There are distinct advantages for representing objects as binary enumerated volumes. Kaufman [10] has called this general approach to representing objects within the context of computer graphics, *volume graphics* and he has compared the pros and cons of the conventional polygon approach to modeling objects to that of volume graphics. One of the present disadvantages of enumerated volumes is that standard polygon renderings appear "blocky" and have a distinct discrete appearance to them that techniques such as smooth shading cannot eliminate. Cohen-Or et al. [2] suggest smoothing out the edges of binary models by using trilinear interpolation (or higher order interpolation)

on the boundary voxels. Here, we take a somewhat different approach. We draw upon the basic ideas and concepts of variational surface design [8, 28] to describe new techniques for computing triangular mesh surfaces that surround an enumerated volume. These triangular mesh surfaces have the same topology as an isosurface computed by a modification of the marching cubes method applied to a field function which has the value one at lattice points lying in the volume and a value of zero for points exterior to the volume. The actual positions of the vertices along these edges are determined by iterative methods used to compute a surface which optimizes certain energy functionals. Our general strategy for solving these minimal variation problems is described in Section 2. We require discrete local approximations for the quantities used to characterize the optimal separating surfaces. These are based upon an interesting property of the particular triangular mesh surfaces which result from marching cubes types of algorithms. We prove that every vertex of one of these triangular mesh surface lies at the intersection of two orthogonal planar curves. This allows for energy functionals for planar curves to be lifted to triangular mesh isosurfaces. In particular, this allows us to take advantage of natural parameterizations of planar polygon curves [14] to obtain constrained isosurface fairing methods that are simple, efficient and effective.

2. Definitions and General Optimization Strategy

Given the increments, $\Delta x, \Delta y, \Delta z$ and the integers N_x, N_y, N_z we denote by L, the rectilinear grid consisting of the lattice points

$$\left\{ P_{ijk} = (i\Delta x, j\Delta y, k\Delta z), i = 0, \cdots, N_x; j = 0, \cdots, N_y; k = 0, \cdots, N_z \right\}.$$

An e*numerated volume* is simply a distinguished subset of L we denote by EV. The complement of EV is denoted by $\overline{EV}$ so that we have $L = EV \cup \overline{EV}$.

A *separating surface* for EV is a surface $S(EV)$ such that any path joining a point in EV to a point in $\overline{EV}$ must intersect $S(EV)$.

We are particularly interested in separating surfaces which are triangular mesh surfaces. The *geometry* of a triangular mesh surface S, consists of a list of vertices $V_i = (x_i, y_i, z_i), i = 1, \cdots, N$ and the *topology* consists of a list of triple indices $(n_i, n_j, n_k), n = 1, \cdots, N_T$ indicating that the surface contains the triangles with vertices V_{n_i}, V_{n_j} and V_{n_k}. If V_i is a vertex of S, then the *star* of V_i consists of all triangles of S that include V_i. We denote the star of S by $(V_i)^*$. The list of indices of the vertices of $(V_i)^*$ connected by edges to V_i is called the *contiguity list* which is denoted by $(i)^*$. Sometimes the topology is specified by giving the contiguity list for each vertex rather than the list of triangles. These two methods are equivalent.

We now set out to define a collection of triangular mesh surfaces which separate the points of EV from the points of $\overline{EV}$. We start with $M(EV)$ which we call the *midpoint separating surface*. $M(EV)$ is obtained by computing the isosurface at the threshold value .5 by using the marching cubes method (modified to take care of the hole problem [16, 18]) applied to the *binary field function* $F(x, y, z)$ defined as

$$F(i\Delta x, j\Delta y, k\Delta z) = \begin{cases} 1, P_{ijk} \in EV \\ 0, P_{ijk} \in \overline{EV} \end{cases}. \quad (1)$$

A vertex V_i of $M(EV)$ lies on the midpoint of an edge of the grid L. We denote the endpoints of these edges as $P_{a_i,b_i,c_i} \in EV$ and $P_{\alpha_i,\beta_i,\gamma_i} \in \overline{EV}$ so that

$$V_i = \frac{P_{a_i,b_i,c_i} + P_{\alpha_i,\beta_i,\gamma_i}}{2}, \; i = 1, \cdots, N. \quad (2)$$

We let $\delta = (\delta_1, \cdots, \delta_i, \cdots, \delta_N)$, where $0 \le \delta_i \le 1$ and define $S(EV, \delta)$ to be a collection of triangular mesh surfaces with the same topology as $M(EV)$ and vertices on exactly the same edges of *L* as *M*(*EV*), but with the vertices

$$V_i = \delta_i P_{a_i,b_i,c_i} + (1 - \delta_i) P_{\alpha_i,\beta_i,\gamma_i}, i = 1, \cdots, N \quad (3)$$

that are allowed to be anywhere on the edge.

In the next section, we describe a general approach to measuring the energy of isosurfaces *S* which we denote by $|S|$. We characterize an optimal separating surface as the solution of the optimization problem

$$\textbf{min} \; |S|, \text{ subject to } S \in S(EV, \delta). \quad (4)$$

We use an iterative scheme for computing the extrema for this problem. We start with an initial surface $S^{(0)}$ with $\delta^{(0)} = (\delta_1^{(0)}, \cdots, \delta_i^{(0)}, \cdots \delta_N^{(0)})$ and for $k = 1, \cdots, N$ we sequentially consider the univariate functions

$$h_k^{(0)}(\delta) = \left| S(EV; \delta_1^{(0)}, \cdots, \delta_{k-1}^{(0)}, \delta, \delta_{k+1}^{(0)} \cdots \delta_N^{(0)}) \right|, \; 0 \le \delta \le 1.$$

We use standard univariate minimization techniques to compute an approximate minimizer of $h_k^{(0)}(\delta)$ which we denoted as $\delta_k^{(1)}$. A full sweep over all vertices leads to the next iterate $S^{(1)}$, with $\delta^{(1)} = (\delta_1^{(1)}, \cdots, \delta_i^{(1)}, \cdots \delta_N^{(1)})$. This iteration is continued until

$$\frac{\left\|\delta^{(k)} - \delta^{(k+1)}\right\|}{\left\|\delta^{(k+1)}\right\|} < \varepsilon .$$

This general strategy is further illustrated in the Figure 1.

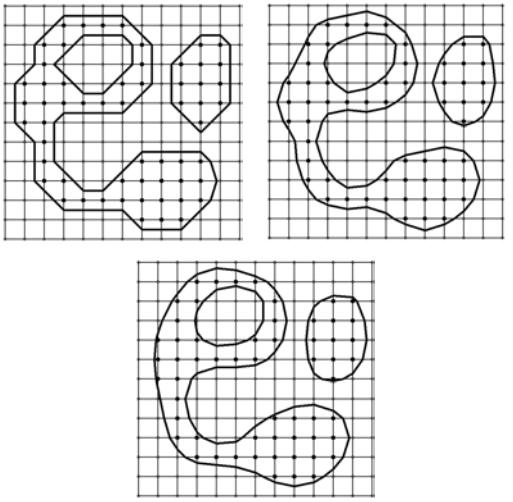

Figure 1: *Top, left image illustrates the 2D version of the enumerated volume and the midpoint separating curve except that the point on the edge joining (11,4) to (12,4) has been moved to its locally optimal position. The top, right image shows the separating polygon after one complete iteration where each edge position has been updated. The lower image shows the final, converged optimal separating polygon curve.*

3. Optimal Separating Surfaces

Our general approach consist of extending optimizing criteria for parametric curves to surfaces by applying a particular curve method to a collection of parametric curves lying on the surface.

We assume at the onset that we have decided upon a measure of smoothness or energy functional for a planar polygon, C, consisting of the vertices $V_1, V_2, \ldots, V_M$. This is written as

$$|C| = \sum_{i=1}^{M} \rho_i(C) \tag{5}$$

where $\rho_i(C)$ is a local, discrete approximation to the energy functional at the point V_i. Any number of choices for the definition of $\rho_i(C)$ are possible. The overall computational efficiency is, of course, dependent upon the ease of computing this local measure of smoothness. One measure used here is based upon curvature

$$\rho_i(C) = \left[\frac{\dot{x}(t_i)\ddot{y}(t_i) - \dot{y}(t_i)\ddot{x}(t_i)}{\left\|\dot{x}(t_i)\right\|^3} \right]^2 . \tag{6}$$

Also, we have used the linearized version of curvature that is often associated with spline functions,

$$\rho_i(C) = [\ddot{x}(t_i)]^2 + [\ddot{y}(t_i)]^2 . \tag{7}$$

The actual computation $\rho_i(C)$ in these cases requires some type of approximation for $(x(t), y(t))$. A reasonable choice is a parametric quadratic polynomial with $(x(0), y(0)) = V_{i-1}$, $(x(t_i), y(t_i)) = V_i$, $(x(1), y(1)) = V_{i+1}$ and $0 < t_i < 1$. A cubic spline is also possible at some additional computational cost.

We now set out to show how to extend the concept of an energy functional for a curve to an isosurface in $S(EV, \alpha)$. We first need the results of the following theorem.

Theorem 1. (**4*-Network**) Let $S \in S(EV, \alpha)$ and consider the planar slices of *S*

$$C_{i\Delta x} = S \cap \{ (x, y, z) : x = i\Delta x \}, i = 0, \cdots, N_x ,$$

$$C_{j\Delta y} = S \cap \{ (x, y, z) : y = j\Delta y \}, j = 0, \cdots, N_y ,$$

$$C_{k\Delta z} = S \cap \{ (x, y, z) : y = k\Delta z \}, k = 0, \cdots, N_z .$$

i) These three collections form a mutually orthogonal network of planar, polygon curves lying on the surface *S*.

ii) Each vertex $V_i \in S$ is at the intersection of exactly two of these planar polygons; one from one of the collection of planar curves and the other from a collection that is orthogonal to it. More precisely,

$$\begin{aligned} &\{ V_n \in C_{i\Delta x} \} \cup \{ V_n \in C_{j\Delta y} \} = \\ &\{ V_n \in C_{k\Delta x} \} \cup \{ V_n \in C_{j\Delta y} \} = \\ &\{ V_n \in C_{i\Delta x} \} \cup \{ V_n \in C_{k\Delta y} \} = \{ V_i, i = 1, \cdots, N \} . \end{aligned} \tag{8}$$

Proof. First, let V_i be an arbitrary vertex of *S* and consider the application of the mc algorithm to a voxel that contains the edge that contains this vertex. Since the fragments of the surface, *S*, lying in a particular voxel are guaranteed to separate the points below the threshold from the points above the threshold, we can be sure that whenever there is a vertex on an edge of the voxel, there will be an edge of *S* on the two faces containing this edge. One of these faces is in a plane perpendicular to the *x*-, *y*- or *z*-axis and the other plane is orthogonal to it. *S* restricted to a plane perpendicular a coordinate axis is a polygon curve which must separate the voxel vertices in the plane which are above the threshold from those that are below the threshold. Since the voxel data we are considering is binary, then the above is true for all *S* in $S(EV, \delta)$. In the

example of Figure 2b, the polygons of $C_{i\Delta x}$ have been colored red, those of $C_{j\Delta y}$ are colored white and those of $C_{k\Delta z}$ are colored blue. The valence of each vertex in the 4*-network is always four (except on the boundary) and the polygon patches are those provided by the various cases of the mc algorithm used.

We should note that above theorem assumes that we are using a modified version of the mc algorithm which corrects the hole problem and guarantees this separation property without adding triangles on faces of voxels. The method of Nielson & Hamann [16] guarantees these properties as does the method described by Nielson & Huang [18].

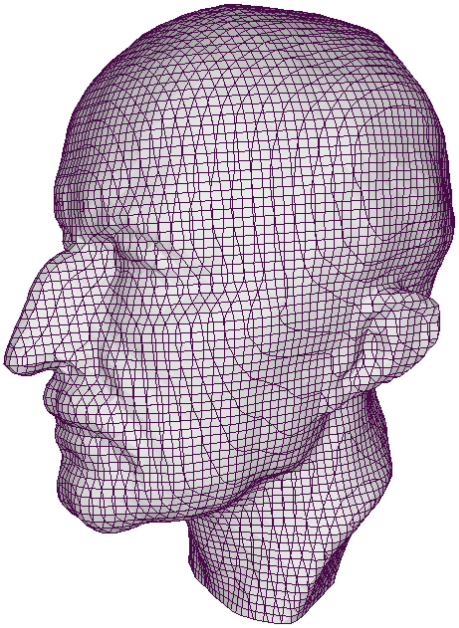

Figure 2a: *Max Planck bust with 4*-network.*

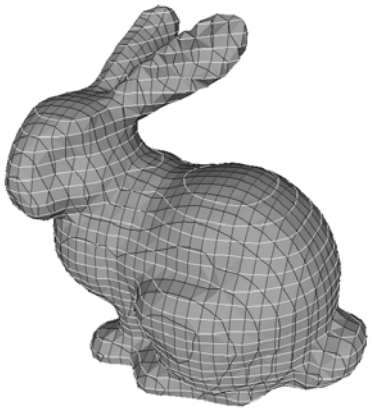

Figure 2b: *The three families of orthogonal planar curves comprising the 4*-network of the isosurface.*

The importance of the above theorem in the present context is the following. Obtaining a good global parameterization of a triangular mesh surface is currently still a somewhat difficult problem, but it is an easy matter to parameterize the components of a planar polygon curve [14] and use this parameterization to obtain local discrete approximations to energy functionals. We can use these observations to lift the concept of a measure of smoothness for a planar curve to a an isosurface in $S(EV,\delta)$ by the following

$$|S| = |S(EV,\alpha)| = \sum_i |C_{i\Delta x}| + \sum_j |C_{j\Delta y}| + \sum_k |C_{k\Delta z}| \quad . \quad (9)$$

4. Examples and Applications

4.1 Knotted Tori

A torus is an interesting example since it contains points with positive (elliptic) , negative (hyperbolic) and zero (parabolic) Gaussian curvature. For this example we computed the points of a $24 \times 24 \times 24$ grid lying interior to one of two tori which are topologically linked. The midpoint separating surface is shown in Figure 3a. After one complete iteration, the surface shown in Figure 3b is obtained. The final converged surface is shown in Figure 3c.

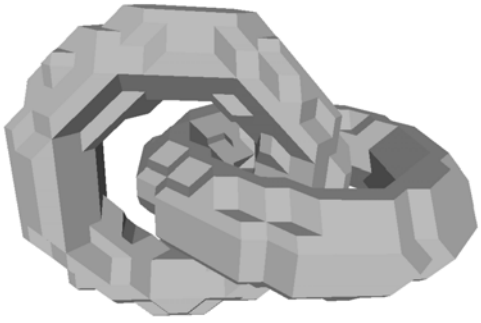

Figure 3a: *EV of points in one of two tori.*

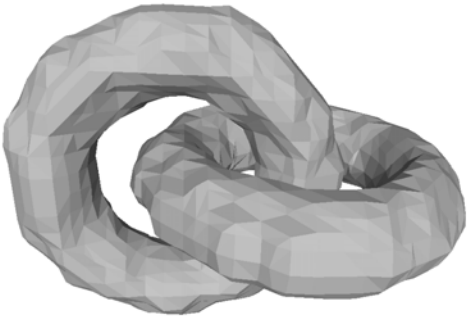

Figure 3b: *One complete iteration.*

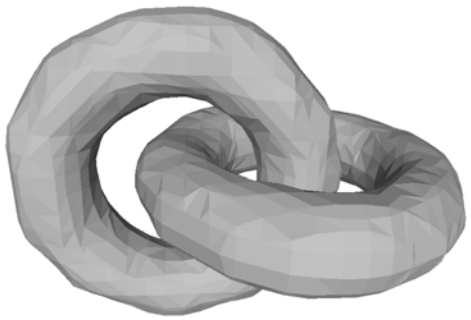

Figure 3c: *The limiting optimal separating surface.*

4.2 Boolean Operations on Triangular Mesh Surfaces

While it usually considered a difficult task to perform Boolean operations on surface bounded objects, it is trivial for enumerated binary volumes. For this example we started with a triangular mesh surface of the Stanford bunny data set. We then computed a binary enumerated volume for the Stanford bunny by selecting the distinguished subset of a $60 \times 60 \times 60$ lattice of points lying interior to the bunny. This enumerated bunny volume was then intersected with an enumerated volume for the block letters "ASU". Figure 4a shows the raw data by displaying the midpoint surface shrouded over the intersected enumerated volume. Figure 4b shows the initial guess consisting of random positions on the edges of $S(EV, \delta)$. Figure 4c shows the triangular mesh surface after one full sweep iteration. We have used a random initial approximation to point out the insensitivity of our optimization strategy to initial approximations. We have observed that most often the final optimal separating surface is independent of the initial approximation. While we have observed cases where different initial values have converged to different surface, usually these cases were small, symmetric and somewhat contrived data examples or extreme cases where $\delta_i^{(0)} = 0 \text{ or } 1$. While we do not rule out the possibility of local extrema, experience to date tells us it is not a problem in this context.

Figure 4a: *Midpoint surface of enumerated volume data.*

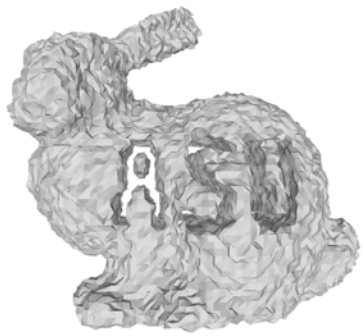

Figure 4b: *Random initial approximation.*

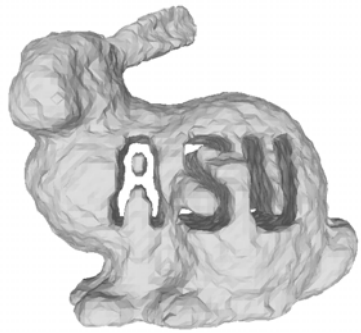

Figure 4c: *One iteration from a random initial approximation.*

Figure 4d: *Optimal separating surface.*

4.3 Compression of Isosurfaces

In this section we discuss an interesting application of the present methods to compressing the representation of geometric objects. Compressing triangular mesh surface is a topic that has received considerable research attention in recent times. The methods we describe here are quite effective, but only apply to isosurfaces extracted from volume data sets using a mc type of algorithm. As we noted in Section 1, there are two separate aspects of a triangular mesh surface; namely the topology and the geometry. In the present situation, where the surface is a

mc isosurface, the topology is completely determined by the binary field function,

$$F(i\Delta x, j\Delta y, k\Delta z) = F_{ijk} = \begin{cases} 1, P_{ijk} \in EV \\ 0, P_{ijk} \in \overline{EV} \end{cases}.$$

The binary array F_{ijk} is also called the *occupancy array*. Using standard and widely available techniques, it is possible to efficiently encode this topological information. For example, binary image compression techniques can be applied to the 2D layers of F_{ijk}. The JBIG algorithm is a context based arithmetic coding scheme which forms the bases of the standard of the Joint Bi-level Image experts Group [29]. Taking into consideration potential interlayer context, Taubin reports .60 to .95 bits/triangle being about 50% better than just applying JBIG to isolated layers [25]. Saupe and Kuska, further involve octrees in order to exploit spatial coherence for added efficiency [23].

The geometry for the isosurface requires the values α_i of

$$V_i = \delta_i P_{a_i,b_i,c_i} + (1-\delta_i) P_{\alpha_i,\beta_i,\gamma_i}, i = 1, \cdots, N .$$

An approximation to the surface results from quantizing these values. Using M-bits, the interval $[0,1]$ is subdivided into 2^M subintervals and δ_i is approximated with the midpoint of subinterval closest to δ_i. Each bit-plane of these quantized values can then be encoded and compressed with techniques similar to those used for the topology. This brings us to how the present techniques are applicable in this context. If the isosurface is expected to be relatively smooth, then a smaller number of bits can be used for quantizing the geometry and the surfaces can be faired using the present methods. The vertices are constrained to the subinterval specified by the quantizing process. This approach is illustrated in the example of Figure 5 where we start with an enumerated volume of size $100 \times 300 \times 100$. For some applications, an approximation of the quality shown in the right image of this Figure 5a may be sufficient. This requires no information beyond the topology. The smooth quality is gained through the optimization process used to compute the shroud. While the shroud adds no additional cost in space, there is the cost required for computing the $\delta_i's$ of the optimal surface. It depends upon the application and the efficiency of the implementation as to whether or not the archiving or bandwidth costs are sufficient to justify the smoothing costs. In most situations, this decision would require additional study. The model of the left image of Figure 5b is optimized after 1-bit of quantification and the right uses 2-bits. All four models have the same topology with approximately 100K triangles. The two models of Figure 5a can be represented with approximately 50K bits. The left model of Figure 5b requires approximately 150K bits and the right about 250K bits.

Figure 5a: *The enumerated volume of size* $100 \times 300 \times 100$ *and its optimal shroud.*

Figure 5b: *Quantized to 1-bit and 2-bit and then optimized.*

4.4 Segmented Data

Segmentation is one of the steps along the path to extracting meaningful knowledge from acquired data. The actual term *segmentation* is usually used for medical or life science data where it means the process of identifying which pixels or voxels from an image or 3D scan belong to a particular object, such as air, bone, fat or tissue. The term *classification* is also used for this same process. It is not easy to segment data, particularly 3D data. The development of effective segmentation techniques is currently a very active area of research [9, 11, 26]. Often, there is only one material or class to segment and in this case segmented data is exactly the same as an enumerated volume and so the rendering and representation problems are the same. We illustrate the use of our techniques in this context with two examples. They both use data from our NSF sponsored, interdisciplinary research project at ASU: *3D Knowledge: Acquisition, Representation and Analysis*.

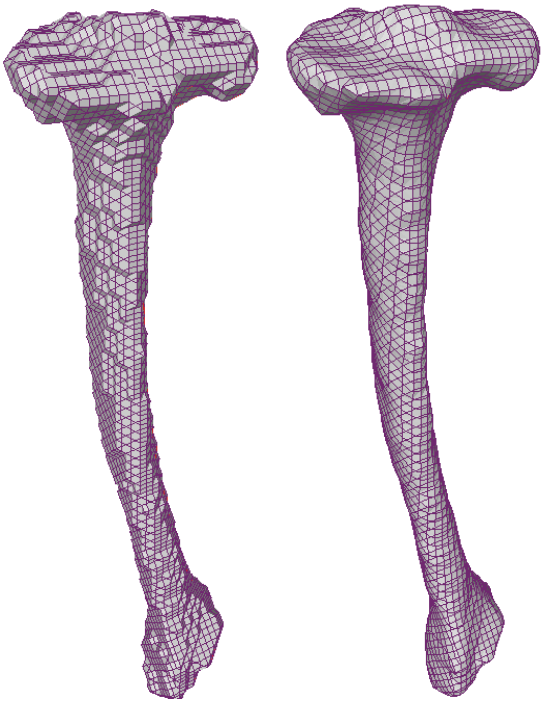

Figure 6: *The left image is the midpoint surface defining segmented data of size* $32 \times 96 \times 32$ *of a right tibia from a male Pan troglodytes (chimpanzee). The right image is the optimal shroud with its 4*-network.*

The data from the first project, which is shown in Figure 6, is concerned with understanding the abilities, limitations, and adaptations of early humans to make tools and walk upright by developing biomechanical models of manipulative and locomotor behavior using 3D osteologoical data. Quantifying the morphology of certain features and attributes developed through the evolutionary process is key to understanding why and how these features evolved. This quantification requires mathematical models of the surfaces of segmented objects. While most other applications we have discussed so far utilize the shroud for rendering, here we can see that the smoothed isosurface can be used to extract key geometric and quantifiable features such as the area of regions of positive and negative curvature or contact area.

This next example utilizes data from another one of our interdisciplinary 3DK research projects. Extraction of scaffolds, such as the meiotic spindles, a 3D tubular framework consisting of the microtubules, from confocal laser scanning microscopy (CLSM) data of a cell is a challenge in biological image processing. It is of major importance in the research of microtubule anchor proteins, and molecular motor mechanics. However, the scaffold is hidden with CLSM data due to the nature of light excitation, and is difficult to visualize using traditional opacity and color transfer functions that depend only on local intensity. In [9], a new method of segmenting this type of data which is based upon statistical methods utilizing crest points is described. Once the scaffold has been extracted, this binary volume can be modeled and rendered with an optimal shroud. This is illustrated in Figure 7. The filtered spindle is segmented, producing an enumerated volume size $29 \times 121 \times 28$.

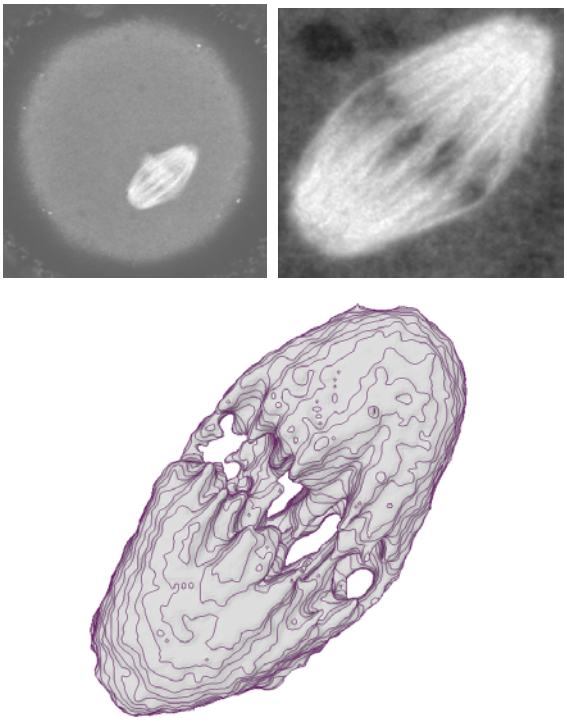

Figure 7: *The top, left image is confocal microscope data. The top right image is a volume rendering and the bottom image is the shroud surface for the filtered, segmented meiotic spindle with contours to show fairing results.*

The next example is segmented data of a human brain [11, 26]. We show this data in Figure 8a by displaying the midpoint separating surface. The optimal shroud converges in four iterations to approximately 6-digit accuracy. It is shown in Figure 8b. Another view of the shroud is shown in Figure 8c. Here we can see the region where a tumor has been removed, but the main reason we show this view is that the quality of the smoothing is clearly discernable from the axial contours.

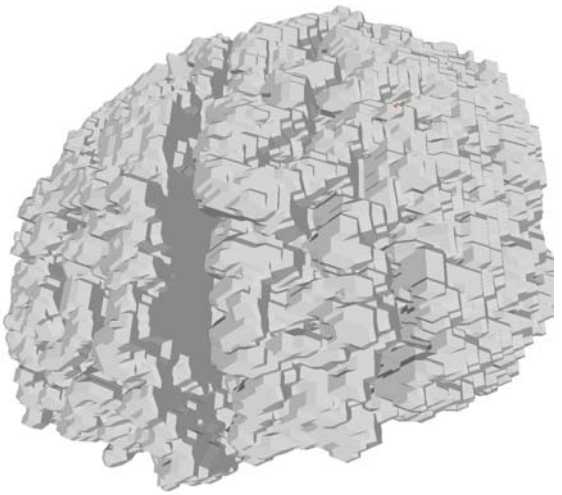

Figure 8a: *Segmented brain data of size* $124 \times 256 \times 256$ *illustrated with the midpoint separating surface,* $M(EV)$.

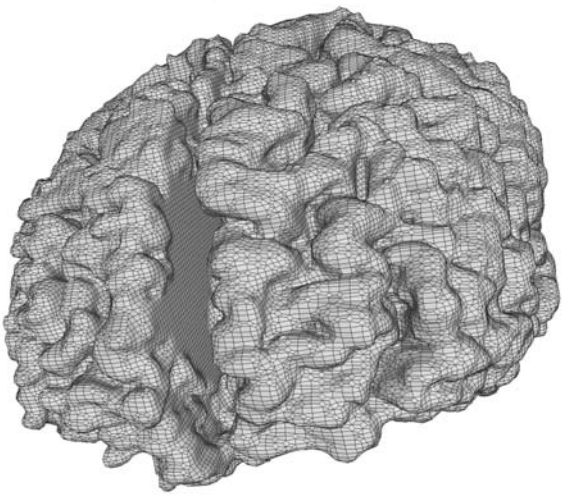

Figure 8b: *Optimal shroud of the data of Figure 8a.*

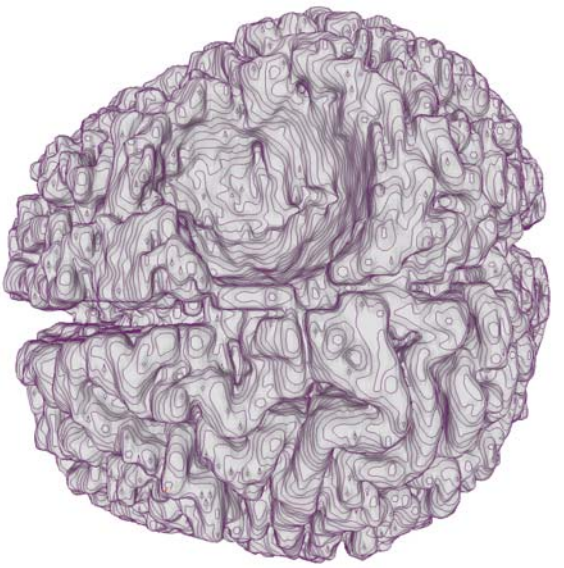

Figure 8c: *Top view with tumor cavity in view and contours illustrating the quality of the fairing process.*

4.5 Target Containment Region Description

One of the most common sensors used on modern submarines is the towed array (TA), a linear string of hydrophones towed behind the parent submarine. Directional beams are developed electronically and sound from a target is processed through one of these beams. The array construction and electronic processing results in conical beams of known angular width centered about the axis of the TA and extending in all directions. If target noise is received in one of these beams it is known that the target is contained somewhere in the conic annulus of the received beam. If sound from the target is received at the TA after bouncing off the ocean floor, the containment annulus now includes the hyperbolic sheet resulting from the beams' reflection off the bottom. Figure 9 illustrates the basic geometry of this problem. A variety of factors can affect this ideal situation. For example when the bathymetry of the seafloor and nonlinear acoustic propogation are taken into consideration, a region similar to that depicted in Figure 10 can result. Given estimates of the speed of the target, it is possible to update the containment region by enlarging it with offsets. New observation at a latter time would lead to new containment region found by intersecting containment regions. Dynamically maintaining a geometric region of this nature with a polygon bounded surface would be a difficult task requiring real-time offset and intersection capabilities. We have used enumerated volumes to model these containment regions. In order to enhance the visual display of this information to fire control operators, the shroud can used. An example is shown in Figure 11.

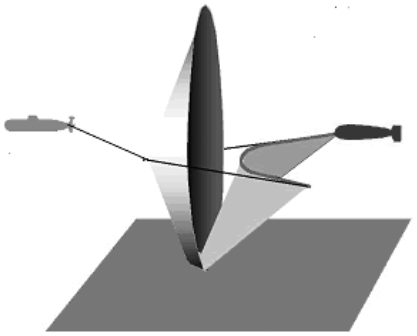

Figure 9: The basic geometry of towed sonar data. From the data, a point on the target (right submarine) is known to be in the reflected annulus. Image is courtesy of K. Lima & R. Shell, Naval Undersea Warfare Center, Newport.

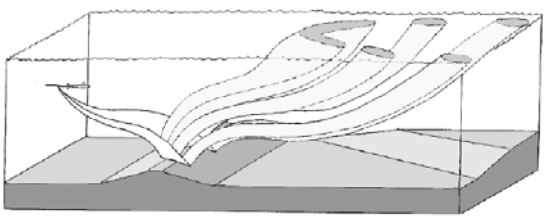

Figure 10: *The effect of the seafloor bathymetry on the containment region. Artistic rendition by William Gilroy, NUWC.*

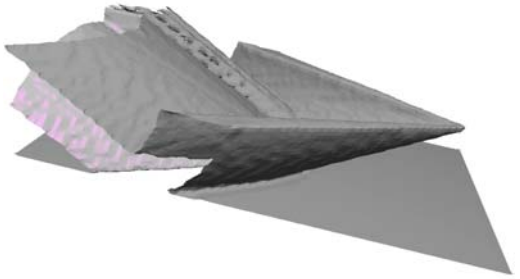

Figure 11: *Target containment region modeled as enumerated volume and displayed with optimal separating surface.*

5. Remarks

1. All of the images we have included here use constant (flat) shading. The main reason for this is because the geometry of the triangular mesh surface is best revealed without the additional enhancement of Gouraud (smooth) shading. Also, we found that specular reflection added very little to what we wished to impart and so we used only the ambient and diffuse components of the Phong illumination model.

2. We have experimented with a variety of choices for the local energy functional, $\rho_i(C)$, including the definitions of (6) and (7), combinations of these two and even some ad hoc schemes involving the angles $\angle V_{i-1}V_iV_{i+1}$. In general, practically any reasonable choice for $\rho_i(C)$ leads to somewhat reasonable results. This is due, in part, to the constraints placed on the vertices during the optimization process. In some applications, certain choices clearly give superior results. Of course, what is superior in any particular application is a subjective matter. We found that a test bed environment with a variety of choices for $\rho_i(C)$ available, usually allows a user to find quit rapidly a criterion suitable for a particular application. This points out one of the advantages of our general approach. Any measure of smoothness for a planar polygon can easily and readily be lifted to isosurfaces and plugged into our general optimization strategy. This leads to a variety of future possible research problems. We are currently working on variational criteria that additionally enforce certain constraints such as creases or other related aspects. Another energy functional that we plan to study is

$$\rho_i(C) = [\ddot{x}(t_i)]^2 + [\ddot{y}(t_i)]^2 + \nu_i\left\{|\dot{x}(t_i)|^2 + |\dot{y}(t_i)|^2\right\}$$

which is associated with splines in tension.

3. The optimal separating surfaces developed here are 2D manifolds which means that each edge of *S* is shared by, at most, two triangles. This is not the case for the methods of [1, 6, 15]. By design, the methods of [1, 15] will separate more than two materials so they necessarily cannot be 2D manifolds. It would be interesting to extend the ideas of an optimal shroud to the case of several materials to be separated.

Acknowledgements

The original idea of this research topic came from an ONR sponsored research project (N00014-00-1-0281) working with the Naval Undersea Warfare Center on the development of the TALOSS system. We also wish to acknowledge the support of the National Science Foundation (NSF IIS-9980166 & ACI-0083609) and DARPA (MDA972-00-1-0027). We wish to thank Drs. Simon Warfield, Michael Kaus, Ron Kikinis, Peter Black and Ferenc Jolesz for sharing the tumor database. The data for the bunny and the statue of David are courtesy of Stanford University. The Max Planck data is courtesy of Leif Kobbelt, Aachen. The chimp bone data is courtesy of Mary Marzke, ASU. The mouse egg data is courtesy of Dave Capco, ASU.

References

1. K. S. Bonnell, D. R. Schikore, K. I. Joy, M. Duchaineau & B. Hamann, Constructing material interfaces from data sets with volume-fraction

information, In *Proceedings of Visualization '00*, pp. 367-372, IEEE Press, 2000.

2. D. Cohen-Or, A. Kadosh, D. Levin & R. Yagel, Smooth boundary surfaces from binary 3D datasets, in: *Volume Graphics*, M. Chen, A. E. Kaufman, R. Yagel (eds.), pp. 71-78, Springer, 2000.
3. M. Desbrun, M. Meyer, P. Schroeder and A. Barr, Implicit fairing of irregular meshes using diffusion and curvature flow, In *Proceedings of SIGGRAPH* '99, pp. 317-324, 1999.
4. M. Desbrun, M. Meyer and P. Alliez, Intrinsic parameterizations of surface meshes, Eurorgraphics 2002, Computer Graphics Forum, Vol. 21, No. 2, pp. 666-911, 2002.
5. N. Dyn, K. Hormann, S-J. Kim and D. Levin, Optimizing 3D triangulations using discrete curvature analysis, in: *Mathematical Methods for Curves and Surfaces Oslo 2000*, T. Lyche & L. L. Schumaker (eds.), pp. 135-146, Vanderbilt University Press, 2001.
6. S. Frisken, Constrained elastic surface nets: generating smooth surfaces from binary segmented data. MICCAI, pp. 888-898, 1999.
7. A. Gray, *Modern Differential Geometry of Curves and Surfaces*, CRC Press, 1998.
8. H. Hagen, S. Hahmann, G. P. Bonneau, Variational surface design and surface interrogaton, In *Proceedings of Eurographics '93*, Computer Graphics Forum 12 (3), pp. 447-459, 1993.
9. J. Hu, P. D. Baluch, A. Razdan, G. M. Nielson, G. E. Farin and D. G. Capco, Case study: Cellular scaffold extraction using crest point for volume rendering, VisSym '03, Eurographics Association, 2003.
10. A. E. Kaufman, State-of-the-art in volume graphics, in: *Volume Graphics*, M. Chen, A. E. Kaufman, R. Yagel (eds.),pp. 71-78, Springer, 2000.
11. M. Kaus, S. K. Warfield, A. Nabavi, P. M. Black, F. A. Jolesz, and R. Kikinis, Segmentation of MRI of Brain Tumors, *Radiology,* Vol. 218, pp. 586-591, 2001.
12. L. Kobbelt, Discrete fairing, In *The Mathematics of Surfaces VII*, T. Goodman and R. Martin (eds.), Clarendon Press, Oxford, pp. 101-131, 1997.
13. W. E. Lorensen and H. E. Cline, Marching cubes: A high resolution 3D surface construction algorithm, In *Proceedings of SIGGRAPH '87*,pp. 163-169, 1987.
14. G. M. Nielson and T. Foley, Knot selection for parametric spline interpolation, In *Mathematical Methods in Computer Aided Geometric Design*, T. Lyche and L. Schumaker (eds.), Academic Press, pp. 261-271, 1989.
15. G. M. Nielson and R. Franke, Computing the separating surface of segmented data, In *Proceedings of Visualization '97*, pp. 229-233, IEEE Press, 1997.
16. G. M. Nielson and B. Hamann, The asymptotic decider: Resolving the ambiguity in marching cubes, In *Proceedings of Visualization '91*, pp. 83-91, 1991.
17. G. M. Nielson, Volume modeling, In *Volume Graphics*, M. Chen, A. E. Kaufman, R. Yagel (eds.), Springer, 2000.
18. G. M. Nielson and A. Huang, Approximating normals for marching cubes applied to locally supported isosurfaces, In *Proceedings of Visualization '02*, pp. 459-466, 2002.
19. Y. Ohtake & A. G. Belyaev, Mesh optimization for polygonal isosurfaces, Computer Graphics Forum, Vol 20, No. 3, pp. 368-276, 2001.
20. U. Pinkall & K. Polthier, Computing discrete minimal surfaces, *Experimental Mathematics*, Vol. 2, No. 1, pp. 15-36, 1993.
21. K. Polthier, Polyhedral surfaces of constant mean curvature, Habilitationsshcrift, Technische Universität Berlin, 2002.
22. M. Rumpf, A variational approach to optimal meshes. *Numer. Math*., Vol. 72, pp. 523-540, 1996.
23. D. Saupe and J.-P. Kuska, Compression of isosurfaces, In *Proceedings of IEEE Vision, Modelling and Visualization* (VMV 2001) Stuttgart, 2001.
24. G. Taubin, A signal processing approach to fair surface design, In *Proceedings of SIGGRAPH '95*, pp. 351-358, ACM Press, 1995.
25. G. Taubin, BLIC: Bi-level isosurface compression, In *Proceedings of Visualizaton '02*, pp. 451-458, IEEE Press, 2002.
26. S. K. Warfield, M. Kaus, F. A. Jolesz, and R. Kikinis, Adaptive, Template Moderated, Spatially Varying Statistical Classification, *Med Image Anal*, Vol.4, No.1, pp. 43-55, 2000.
27. K. Weinstein, Scanline surfacing: building separting surfaces from planar contours, In *Proceedings of Visualization '00*, pp. 283-289, IEEE Press, 2000.
28. W. Welch & A. Witkin, Free-from shape design using triangulated surfaces, In *Proceedings of SIGGRAPH* '94, pp. 247-256, ACM Press, 1994.
29. *Progressive bi-level image compression - Coded representation of picture and audio information - Information Technology*, Recommendation T.82, International Telecommunication Union, Geneva, March, 1993.

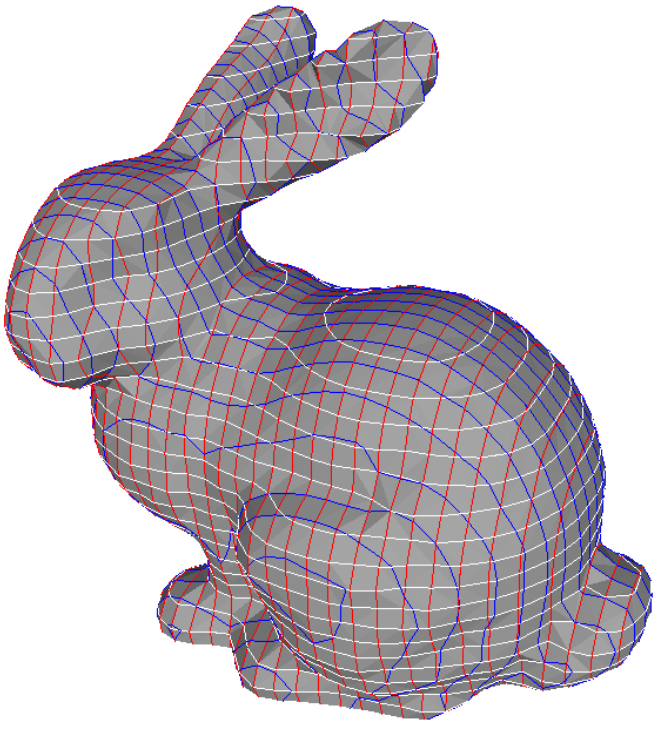

Figure 2b: *The three families of orthogonal planar curves comprising the 4*-network of the isosurface.*

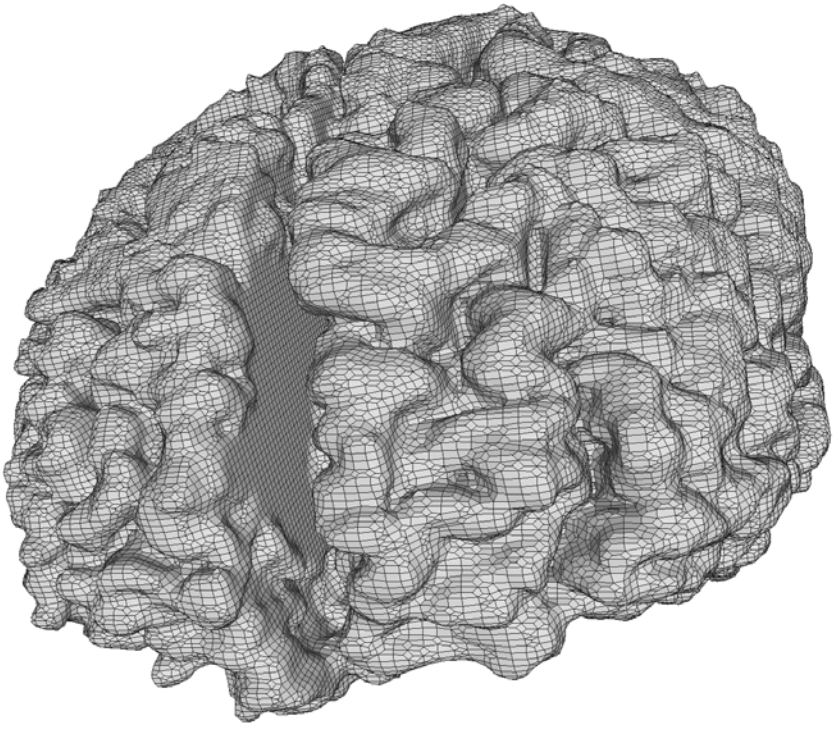

Figure 8b: *Optimal shroud of the data of Figure 8a.*